Model for the radial distribution function of polydisperse inertial spheres settling in homogeneous, isotropic turbulence

Johnson Dhanasekaran
Sibley School of Mechanical and Aerospace Engineering, Cornell University, Ithaca, New York 14853, USA

Donald L. Koch*
Smith School of Chemical and Biomolecular Engineering, Cornell University, Ithaca, New York 14853, USA

(Received 18 April 2022; accepted 21 September 2022; published 7 October 2022)

While particle inertia is widely known to cause substantial clustering of monodisperse particles in turbulent flows, differential sedimentation of polydisperse particles can rapidly decorrelate their relative positions and attenuate clustering. This paper presents a simple analytical model for the radial distribution function (RDF) of inertial particles settling in homogeneous, isotropic turbulence over a broad range of particle Stokes numbers, settling parameters, size ratios, and interparticle separations. We first draw on previous theories and direct-numerical simulations (DNS) to develop a simple comprehensive fit for the RDF of monodisperse particles without sedimentation. Even in the absence of gravity, the relative positions of polydisperse particles decorrelate as a result of turbulent accelerations, which have been treated as an acceleration-driven relative diffusivity of unequal size particles balancing the radial diffusion and drift resulting from turbulent shearing motions. We develop a similar model to describe the orientational averaged pair distribution function or RDF in the presence of differential sedimentation. The model is validated by comparison with DNS results for polydisperse settling particles. Juxtaposition of the model predictions with a variety of experimental measurements provides a perspective on current empirical knowledge of the RDF of sedimenting particles in turbulence. A sample calculation is then performed to illustrate the effect of preferential concentration in the presence of differential sedimentation on the coalescence rate of cloud droplets.

DOI: 10.1103/PhysRevFluids.7.104602

I. INTRODUCTION

Particle inertia causes a delay in the particle's response to a background turbulent gas velocity field. This leads to accumulation in certain regions of the flow causing a local enhancement in particle concentration, a higher probability of other particles in the neighborhood of any particle, and an increased probability of particle collisions. Thus, particle inertia, through concentration enhancement, can significantly influence the evolution of the size distribution of coalescing drops or coagulating particles even when its direct effect on collision dynamics is negligible. Particle inertia is expected to cluster droplets with radii of $O(10\mu\text{m})$ in clouds [1] and so cloud models will require input concerning the degree of concentration enhancement. Differential sedimentation resulting from polydispersity rapidly attenuates particle clustering [1]. Current analytical results are inadequate to describe particle clustering across the relevant parameter space and very limited direct numerical simulation (DNS) results are available. This paper presents a model that quantifies the competing effects of differential sedimentation decorrelation and turbulence on particle clustering.

*dlk15@cornell.edu

This result will directly inform evolution of micron-sized droplets in clouds, where both differential sedimentation and turbulence are expected to be important. Inertial clustering is also expected to play a role in protoplanetary disks increasing the probability of planetesimal formation [2]. The accuracy of astrophysical models of this phenomenon could be improved using the outcome of our study. Other potential applications include aggregation driven growth of commercially valuable products in industrial reactors and agglomeration of pollutants in air.

We will begin by considering a monodisperse suspension in the absence of gravity. In this case, the Stokes number is the most important factor influencing inertial clustering. The Stokes number is defined as $\mathrm{St} \equiv \tau_p/\tau_\eta$, the ratio of the particle response time to the fluid timescale. Here $\tau_p = 2\rho_p a^2/(9\mu)$ is the time for a particle of radius a and density ρ_p to change its velocity in response to changes in fluid velocity and μ is the dynamic viscosity. The fluid timescale is typically chosen to be the Kolmogorov timescale $\tau_\eta = (\nu/\epsilon)^{1/2}$, where ϵ is the turbulent dissipation rate, $\nu = \mu/\rho$ is the kinematic viscosity and ρ is the density of the gas. In the low St limit, particles nearly follow the fluid and increases in St above this limit lead to enhanced local particle concentration. In the large St limit particles do not respond to the fluid and this leads to a random distribution of particles and no enhancement of local concentration. Thus, monodisperse particles cluster most strongly at an $O(1)$ value of the Stokes number.

At the present time, the only means of accurately determining the radial distribution function (RDF) $g(r)$ of monodisperse particles over the full range of St and particle separations r is through DNS studies. However, asymptotic results are available for r lying within certain length scale ranges of turbulence [3,4]. In the small St limit, Chun *et al.* and Zaichik and Alipchenkov [3,5] derived an analytical expression for inertial clustering in the dissipative range, $r \ll \eta$, where $\eta = \nu^{3/4}/\epsilon^{1/4}$ is the Kolmogorov length scale. In the inertial subrange, $\eta \ll r \ll L$, Bragg *et al.* [4] obtained a result for small values of the scale dependent Stokes number, defined as the ratio of the particle response time to the turnover time of an eddy of size r. Here, L is the integral length scale. The scale dependent Stokes number is $\mathrm{St}_r \equiv \mathrm{St}(\eta/r)^{-2/3}$ [6]. A result for inertial clustering across the full parameter space can be obtained through the model for the probability distribution of pair relative velocity [5,7,8]. However, Ireland *et al.* [9,10] showed that to accurately predict inertial clustering some of the inputs for this model had to be obtained from DNS. Additionally closed form solutions are available only in certain cases. Solutions of this model for St greater than 0.3 were also shown to be inaccurate due to nonlocal effects [11], where particles are slingshot from one eddy to another. To resolve all of these issues we will develop a closed form expression for $g(r)$, when all the spheres are of equal size, that incorporates many of the important asymptotic results and provides a good fit to the DNS results reported at Re_λ, the Reynolds number based on the Taylor microscale, of 597 [9]. This value of Re_λ is chosen to be as close as possible to the $O(10^4)$ Taylor-scale Reynolds numbers typical in clouds and other real-world turbulent flows. Fortunately, it has been shown that clustering is not very sensitive to Re_λ in the limit of large Re_λ [9]. Thus, our monodisperse inertial clustering result is expected to be accurate over a large range of Re_λ, St, and r.

Multiple DNS studies have examined the role of gravity [10,12,13] in inertial clustering. Gravity influences clustering in two ways: (1) it changes the manner in which the particles sample the flow field; and (2) it induces relative motion between particles of different size decorrelating their positions. A parameter describing the importance of gravitational sampling is the ratio of the particle settling velocity ($U = \tau_p g$) to the Kolmogorov velocity (u_η), $S_v \equiv U/u_\eta$. Here g is the acceleration due to gravity. A particle independent metric is the Froude number $\mathrm{Fr} \equiv \mathrm{St}/S_v = \epsilon^{3/4}/(\nu^{1/4} g)$ capturing the relative importance of turbulent evolution and gravitational sampling. While asymptotically large values of Fr should be required in principle to neglect the impact of settling on turbulence sampling, Dhariwal and Bragg [12] found $\mathrm{Fr} = 0.3$, representative of a high turbulence cloud with $\epsilon = 10^{-1}\ \mathrm{m}^2/\mathrm{s}^3$, to be large enough that gravitational sampling induced distortions of the RDF are negligible. Thus, the relative motion of particles due to differential sedimentation has a much larger impact on the RDF for moderate or large Fr. For smaller Fr the paucity of DNS data and theoretical insight prevents the development of a predictive model at this time. Hence, our model will focus on the role of differential sedimentation in inertial clustering.

Turbulent and gravitational accelerations induce relative motion of particle pairs of different size limiting the degree of preferential concentration of polydisperse particles. The first DNS study to illustrate the dramatic reduction in preferential concentration due to differential sedimentation was presented by Ayala *et al.* [1]. In a follow up article, the same authors provided a fit to the results without attempting to describe the underlying physics [14]. Dhariwal and Bragg [12] performed a more extensive DNS study of inertial clustering of sedimenting bidisperse particles. A mechanistic study of the effects of turbulent acceleration, without gravity, is available for low St particles with separations in the dissipative range [3]. It contains an analytical result obtained by solving a drift-diffusion equation in which turbulent acceleration contributed to the isotropic pair diffusivity. The resulting RDF exhibited a cross-over pair separation above which the inertial clustering behavior is similar to that of a monodisperse system and below which the RDF is insensitive to separation. Lu *et al.* [15] incorporated an estimate of differential sedimentation into this cross-over length to predict inertial clustering in the dissipative range. We improve on this analysis by developing a drift-diffusion equation that is applicable over all the scales of turbulence. The pair diffusion contains a single adjustable constant that is obtained from a comparison with the DNS results of Dhariwal and Bragg [12]. To validate our model we compare against the DNS results of the RDF at particle contact reported by Ayala *et al.* [1] and find good agreement.

Our inertial clustering model is compared with experimental data from multiple studies [16–18]. To account for polydispersity in experiments the RDF is averaged over the reported experimental size distributions. The model predictions agree well with RDFs measured in these experiments and the comparison provides a perspective on where the measurements lie within the range of clustering behaviors one would expect to see based on the currently available theoretical and DNS results that led to the model development. The model does not agree with experimental RDF's measured by Yavuz *et al.* [19] and we argue that these experiments do not exhibit consistent trends across the parameter space that would be expected based on the current understanding of inertial clustering.

As a sample application, we apply the model to predict the coalescence rate of micron-sized water droplets settling in clouds. We use results for the local collision rate that incorporate the competing effects of turbulent shear, differential sedimentation and noncontinuum hydrodynamic interactions derived by Dhanasekaran *et al.* [20] and incorporate inertial clustering by multiplying this rate by the RDF predicted by the present model. We evaluate the resulting collision rate over a range of means and standard deviations of the water droplet radii for typical conditions in a cloud, and report the enhancement due to droplet inertia. We find a significant increase in the observed collision rate for nearly monodisperse drops with a rapid decrease in the enhancement with increased polydispersity. This reinforces the necessity for an accurate consideration of the effects of differential sedimentation decorrelation on inertial clustering to accurately predict coalescence rates.

The paper is organized as follows. We first develop the model and validate it against DNS data in Sec. II. Next we compare the predictions of our model with reported experimental data in Sec. III. Then in Sec. IV we analyze the impact of size and size difference on the computed RDF. For this purpose, we calculate the enhancement in collision rate due to inertial clustering of a polydisperse distribution of micron-sized water droplets in clouds across the parameter space. Finally, in Sec. V we summarize the important findings of our study.

II. INERTIAL CLUSTERING MODEL

The RDF $g_{ij}(r)$ measures the enhancement in the probability of finding particles of species i and j separated by a distance r relative to a randomly distributed bulk. For the sake of convenience whenever the two particles are indistinguishable, i.e., $i = j$, we will denote the RDF as $g(r)$.

We first derive an expression for $g(r)$ for separations r across all the scales of turbulence for the monodisperse case without gravity. This expression will build on known results for particles with separations in the dissipative range and inertial subrange. In the dissipative range, corresponding to $r \ll \eta$, Reade and Collins [21] found a power law for $g(r)$ which was later analytically derived for

$\mathrm{St} \ll 1$ [3,5]. This is given as

$$g(r) = c_0 \left(\frac{\eta}{r}\right)^{c_1}. \tag{1}$$

Here c_0 and c_1 are constants depending only on St. Asymptotic analyses for $\mathrm{St} \ll 1$ demonstrate that $c_1 = c_1^* \mathrm{St}^2$ where c_1^* is independent of St [3]. DNS data over a larger range of St show that c_0 and c_1 are independent of Re_λ [9]. The model of Zaichik and Alipchenkov [7] predicted that the power law for inertial clustering accurately describes $g(r)$ for $r \ll \eta$ when St is below a critical value. Above this critical value, $g(r)$ is constant at small separations due to the ballistic motion of heavy particles over small length and timescales. Their model predicted that $g(r)$ flattens for $\mathrm{St} \geqslant 2$. However, DNS data indicates that $g(r)$ plateaus in the $r \ll \eta$ regime only when $\mathrm{St} \geqslant 10$ [9]. The plateau can be described by setting $c_1 = 0$ in Eq. (1).

The next important result was derived by Bragg *et al.* [4] for separations in the inertial subrange, $\eta \ll r \ll L$. This is given as

$$g(r) = \exp\left[c_3 r^{-\frac{4}{3}}\right]. \tag{2}$$

Here c_3 is a constant that depends on St and is set by the difference between the average strain rate and rotation rate experienced by the particles. This result is valid for $\mathrm{Re}_\lambda \to \infty$ and $\mathrm{St}_r \ll 1$.

While these are closed-form expressions within the dissipative regime and inertial subrange there is, to the best of our knowledge, no closed-form equation spanning all separation for which $r \ll L$ including the cross-over between dissipative and inertial ranges. Hence, we propose an expression that incorporates the asymptotic behavior in the dissipative regime and inertial subrange and is consistent with available DNS data [9]. This is given as

$$g(r) = \exp\left(\frac{\log c_0}{\left(1 + \frac{r}{2\eta(1+\mathrm{St}^{3/2})}\right)^{\frac{4}{3}}}\right)\left(1 + \frac{\eta}{r}\right)^{c_1}. \tag{3}$$

The constants c_0 and c_1 depend only on St and can be obtained from DNS data. Data is available spanning St from 0.05 to 30 and we have fitted the constants with this nondimensional number for ease of use. The resulting expressions are given as

$$\begin{aligned} c_0 = 1 + \exp[&0.0005\,\mathrm{St}^7 - 0.0042\,\mathrm{St}^6 - 0.0060\,\mathrm{St}^5 + 0.0803\,\mathrm{St}^4 \\ &+ 0.0030\,\mathrm{St}^3 - 0.7018\,\mathrm{St}^2 + 0.4144\,\mathrm{St} + 1.8686], \end{aligned} \tag{4}$$

$$c_1 = \exp[-0.0230\,\mathrm{St}^3 - 0.4411\,\mathrm{St}^2 - 0.2423\,\mathrm{St} - 0.3750]. \tag{5}$$

Utilizing these constants, we compare the RDF predicted by Eq. (3) against the DNS results in Fig. 1 and excellent agreement is observed.

Equation (3) transitions from asymptote (1) in the dissipative range to asymptote (2) in the inertial subrange. However, it does not incorporate any information about separations comparable to the integral length scale. It is expected that $g(r)$ will decay to 1 at these large separations. The inertial subrange result in Eq. (2) naturally transitions to 1 for $r \to \infty$ and hence so does Eq. (3). This adequately describes DNS data for Re_λ as low as 398 for which there is large separation between the length scales of turbulence. Hence, this result will be accurate for typical conditions in clouds, where Re_λ is $O(10^4)$, and many other real-world systems. However, when the separation of scales is not large and the inertial subrange is not fully developed, corresponding to low Re_λ, an explicit reduction of inertial clustering at the integral scale is needed. The RDF $g'(r)$ for the case of not very large L/η is given as

$$g'_{ij}(r) = 1 + (g_{ij}(r) - 1)\exp\left[-\left(\frac{r}{0.6\,L}\right)^2\right]. \tag{6}$$

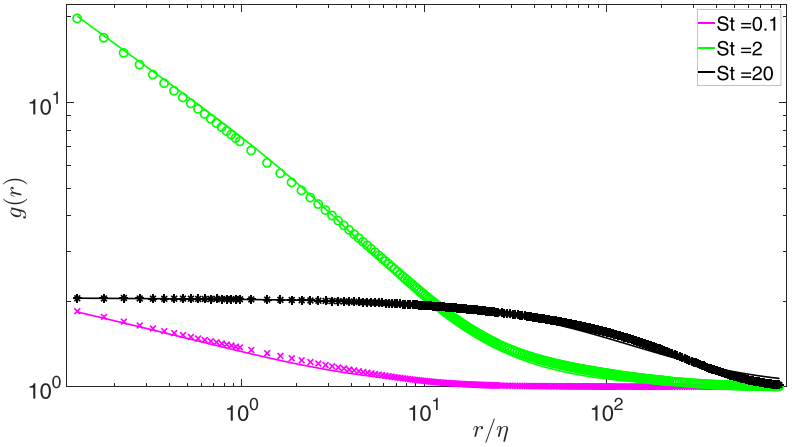

FIG. 1. $g(r)$ is shown as a function of r/η for $\mathrm{Re}_\lambda = 597$ at $\mathrm{St} = 0.1,\ 2,$ and 20 with symbols denoting DNS data [9] and solid lines our model shown in Eq. (3). There is good agreement between the model and DNS results across the parameter space. For $r \ll \eta$, the highest values of $g(r)$ are at the intermediate value of St as expected.

Here, 0.6 is an order one factor that was used to fit the model with DNS data. This quantitatively resolves the RDF for r/η greater than about 10^2 and the qualitative behavior for separations smaller than that. We found this result to be robust even when the particles are not of equal size and it will be applied to the bidisperse results that we derive later in this section. It can be seen that Eq. (6) reduces to Eq. (3) in the limit of large Re_λ, corresponding to large L/η. For some typical values of Re_λ the comparison of DNS data and $g'(r)$ given by Eq. (6) is shown in Fig. 2. In the future discussion, we will not explicitly use primes and will instead note whenever it is necessary to use the expression given in Eq. (6).

The sedimentation of monodisperse particles affects their sampling of the turbulent flow and influences inertial clustering at large values of S_v or equivalently small values of Fr. Through an asymptotic analysis for small St and small Fr, Rani *et al.* [13,22] showed that the RDF in the dissipative range retains the form of Eq. (1) for rapidly setting particles with $c_1 = c_1^* \mathrm{St}^2$ and

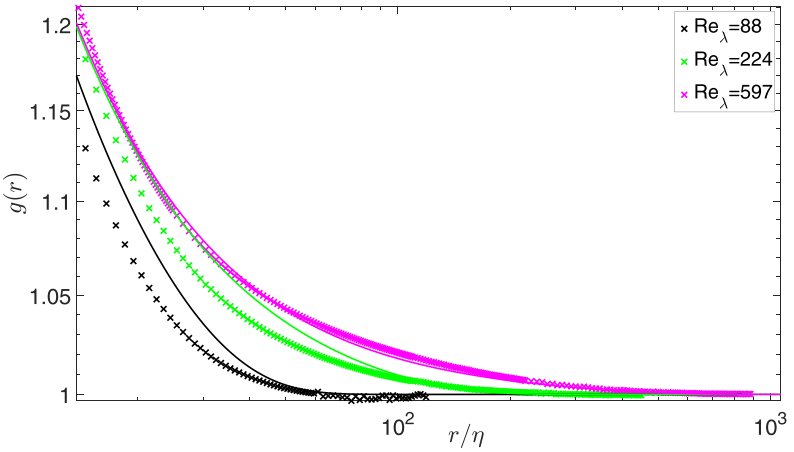

FIG. 2. The RDF is shown as a function of r for $\mathrm{St} = 0.5$ and $\mathrm{Re}_\lambda = 88,\ 224,\ 597$ with symbols denoting DNS data[9] and solid lines the RDF obtained from Eq. (6).

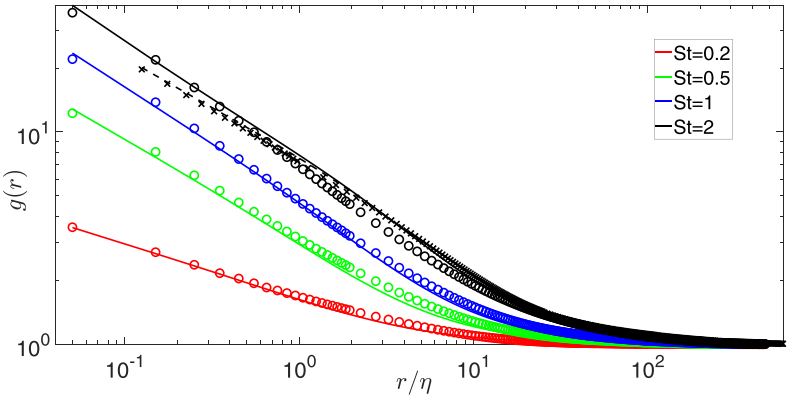

FIG. 3. For monodisperse spheres with St = 0.1, 0.5, 1, 2, corresponding to S_v of 1.9, 9.6, 19.2, 38.5, experiencing gravity along with turbulence, corresponding to Fr of 0.052 and $\mathrm{Re}_\lambda = 398$, $g(r)$ is shown as a function of r/η with symbols(circles) denoting DNS data[10] and solid lines our model shown in Eq. (3). There is good agreement between the model and DNS results across the parameter space. For reference we include the $\mathrm{Re}_\lambda = 597$, St = 2, and $S_v = 0$ DNS ("x") data and our model's prediction (dashed lines) which exhibit only small deviations from the $S_v = 38.5$ results.

a value of c_1^* that is reduced in comparison to the $\mathrm{Fr} = \infty$ asymptote [3]. The DNS determination of the RDF of monodisperse particles at finite Fr is limited to a value of 0.052. The effect of gravity on the RDF at this Froude number remains relatively modest and $g(r)$ in the dissipative range can be fit with Eq. (3) with constants c_0 and c_1, computed over St from 0.05 to 3 given by

$$c_0 = 1 + \exp[-0.0282\,\mathrm{St}^3 - 0.2118\,\mathrm{St}^2 + 0.7936\,\mathrm{St} + 1.3664], \tag{7}$$

$$c_1 = \exp[0.0121\,\mathrm{St}^3 - 0.1729\,\mathrm{St}^2 + 0.1915\,\mathrm{St} - 0.5860]. \tag{8}$$

Figure 3 makes the comparison between the model prediction (3) and DNS results for $g(r)$ for $\mathrm{Fr} = 0.052$ at St = 0.1, 0.5, 1, 2 across the full range of interparticle separations. The good agreement observed indicates that the transition from dissipative to inertial-subrange behavior in Eq. (3) may remain accurate independent of the nondimensional settling velocity and Fr. However, at this time, DNS results are not available to indicate how c_0 and c_1 depend on St and Fr over a range of Froude numbers. Comparing S_v of 1.9, 9.6, 19.2, 38.5, with the $S_v = 0$ results in Fig. 1 indicates similar qualitative behavior and quantitative output. For ease of comparison and conciseness we have included the St = 2 and $S_v = 0$ DNS RDF and our model's prediction of it in Fig. 3. Hence, we will base the model on the $\mathrm{Fr} = \infty$ results (4) and (5) in the rest of this study.

Our model for $g(r)$ will be built on the balance of convection and diffusion of particles. The drift-diffusion equation for low St monodisperse particles in turbulence is given as [3]

$$B_{||}\frac{dg(r)}{dr} + V\,g(r) = 0. \tag{9}$$

Here, **B** is the diffusion tensor of the pair of particles due to turbulent shear, with $||$ indicating the component parallel to the line of centers of the particle pair. The relative velocity of the particle **W** has its radial component defined as $W_r = -V$ and so $V > 0$ indicates a net inward drift along the lines of centers. The turbulent shear diffusivity $B_{||}$ can be expressed as [5]

$$B_{||} = S_{||}(r)T_{Lr}(r). \tag{10}$$

Here $\mathbf{S}(r)$ is the Eulerian structure function, defined as the second moment of the relative velocity of the fluid at two positions and one time. $T_{Lr}(r)$ is the Lagrangian timescale of an eddy of size r.

For two particles of different size, an expression similar to Eq. (9) governs clustering and is given as

$$(B_{||} + D_{||,ij})\frac{dg_{ij}(r)}{dr} + V\, g_{ij}(r) = 0. \tag{11}$$

Here the subscripts i and j denote the two species. $D_{||,ij}$ is the radial component of the diffusion due to difference in the particles' responses to accelerations. Turbulent acceleration was considered as the source of this diffusion in the previous literature [3,23]. In our model, we extend this concept to include a diffusive contribution due to differential sedimentation.

The drift velocity and turbulent shear diffusion occur even for equal size particles. We can compute $B_{||}$ from Eq. (10) with information on the turbulent flow properties $\mathbf{S}(r)$ and $T_{Lr}(r)$. These have been calculated for separations across the different scales of turbulence and reported in the literature [5,7]. A uniformly valid expression based on these results is also available [24,25] and will be used in this study. The drift velocity depends on particle size through the Stokes number. In line with a previous analysis [3] we estimate the drift velocity as that based on an average Stokes number $\mathrm{St} = (\mathrm{St}_i + \mathrm{St}_j)/2$ for the particle pair.

For a bidisperse system with low St in the absence of gravity turbulent acceleration induces a relative velocity $|\tau_{p,i} - \tau_{p,j}|\mathbf{A}$, here $\mathbf{A}$ is the turbulent acceleration and $\tau_{p,i}$ and $\tau_{p,j}$ correspond to characteristic timescales for particles of radii a_i and a_j. The fluctuating relative velocity resulting from turbulent acceleration fluctuations leads to an effective diffusivity given as

$$\mathbf{D}_{\epsilon,ij} = (\tau_{p,i} - \tau_{p,j})^2 \int_{-\infty}^{t} \langle \mathbf{A}(\mathbf{t})\mathbf{A}(\mathbf{t}')\rangle dt'. \tag{12}$$

Here, $\mathbf{D}_{\epsilon,ij}$ is isotropic and hence its component along the line of centers of the particles $D_{||,\epsilon,ij}$ can be easily obtained.

Differential sedimentation due to gravitational acceleration, like turbulent acceleration, acts to separate particle pairs with different response times and limit the degree of clustering for nonmonodisperse cases. It will be seen that the effect of this decorrelation on the RDF scales as $\Delta S_{v,ij}\eta/(a_1 + a_2)$, where $\Delta S_{v,ij} = |S_{v,i} - S_{v,j}|$. As a result differential sedimentation can have a large effect on the RDF of particles that are small compared with the Kolmogorov length scale even if S_v is not large enough for sedimentation to influence the sampling of the turbulent flow.

While gravitational acceleration is steady and acts in a single direction leading to an angular dependence of the pair probability, a simple estimate of its effect can be obtained based on an isotropic approximation. When the turbulent shear acts on a particle pair it rotates the pair so that the gravitational acceleration along the line of centers can fluctuate and change sign. In this sense gravity might be modelled in a qualitative way, as suggested by Lu *et al.* [15], as giving rise to an isotropic relative diffusion, $D_{||,g,ij}$, that is given as

$$D_{||,g,ij} = (\tau_{p,i} - \tau_{p,j})^2 \int_{-\infty}^{t} \langle g_r(t) g_r(t')\rangle dt', \tag{13}$$

where g_r is the component of gravity along the lines of centers of the particles. This leads to an estimate of the dispersion due to gravity of

$$D_{||,g,ij} = U_{\mathrm{rel}}^2 \tau_g. \tag{14}$$

Here $U_{\mathrm{rel}} = |\tau_{p,i} - \tau_{p,j}|\, g$ is the relative settling velocity of the particle pair and τ_g, analogous to the turbulent acceleration correlation time, is the correlation time for the component of gravity along the line of centers. While the gravitational force vector is fixed with respect to the laboratory reference frame, its component along the line of centers g_r varies and eventually decorrelates as a result of the angular component of the shear-induced relative diffusion tensor $\mathbf{B}$. Since this angular component

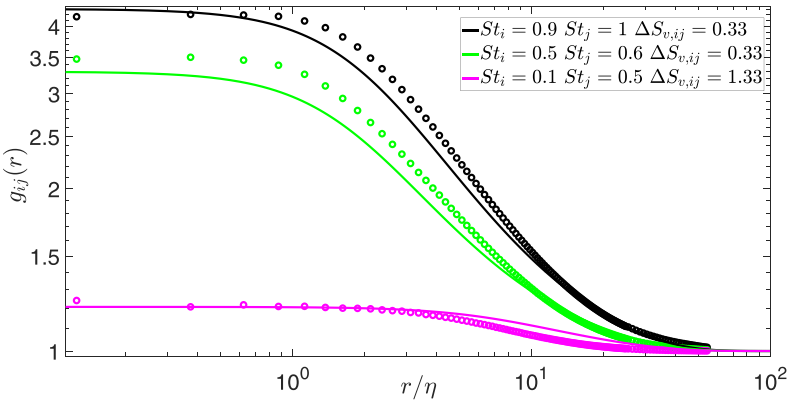

FIG. 4. The RDF for a bidisperse suspension $g_{ij}(r)$ is shown as a function of r/η for three calculations performed at $\mathrm{Re}_\lambda = 90$ and $\mathrm{Fr} = 0.3$. The symbols denote DNS data [12] which are in good agreement with our inertial clustering model indicated by the solid lines.

is of the same order of magnitude as the radial component, we approximate the correlation time as

$$\tau_g = k_g \frac{r^2}{B_{||}}, \tag{15}$$

where k_g is an order one constant. Thus, g_{ij} is given as

$$g_{ij}(r) = \exp\left[\int_r^\infty \frac{V(r')}{B_{||}(r') + D_{||,\epsilon,ij} + D_{||,g,ij}} dr'\right]. \tag{16}$$

To complete the description k_g needs to be determined. This is done by fitting with DNS data[12] and we get

$$k_g = 0.02 + 7.6\left(\frac{\mathrm{St}_i + \mathrm{St}_j}{2}\right)|\mathrm{St}_i - \mathrm{St}_j|. \tag{17}$$

The inertial clustering model we have developed will now be compared with DNS calculations [12] performed at $\mathrm{Fr} = 0.3$ and $\mathrm{Re}_\lambda = 90$. To accurately predict inertial clustering at large particle separations for such a low Taylor-Reynolds number we use the correction for small separation of length scales, given in Eq. (6) on the $g_{ij}(r)$ calculated from Eq. (16). The resulting prediction is plotted in Fig. 4 as a function of the particle pair separation along with DNS data at three sets of Stokes number 0.9–1, 0.5–0.6, 0.1–0.5. Our inertial clustering model, computed using parameters corresponding to high Fr numbers, reproduces the DNS data with high fidelity, including a plateau at small separations caused by differential sedimentation and the variation of the RDF with radial position at larger r due to the inertial drift velocity. The $\Delta S_{v,ij}$ considered here, of $1/3$, $1/3$, and $4/3$, do not greatly alter the sampling of the turbulent velocity field by the particles but they result in sufficient differential sedimentation to significantly reduce the peak clustering. To better understand this we consider $D_{||,g,ij}/B_{||}$, the relative strength of differential sedimentation to turbulent shear. At large separations this parameter, which scales as $\Delta S_{v,ij}\eta/r$, is small. Hence, in the large separations the clustering dynamics is set by the turbulent environment and the RDF resembles the exponential growth seen in Fig. 1. At smaller separations, typically in the dissipative range as r approaches the particle size, $\Delta S_{v,ij}\eta/r$, and by extension $D_{||,g,ij}/B_{||}$, become large and the particle arrangement becomes decorrelated by differential sedimentation thus cutting off the growth in the RDF. With Kolmogorov scales typically on the order of millimetres and particles of about tens of microns even moderately small $\Delta S_{v,ij}$ is enough to generate a large enough $\Delta S_{v,ij}\eta/a$ to flatten the RDF. This is evident in Fig. 6 where $\Delta S_{v,ij}$ as low as $1/3$ can move the RDF away from the monotonic behavior.

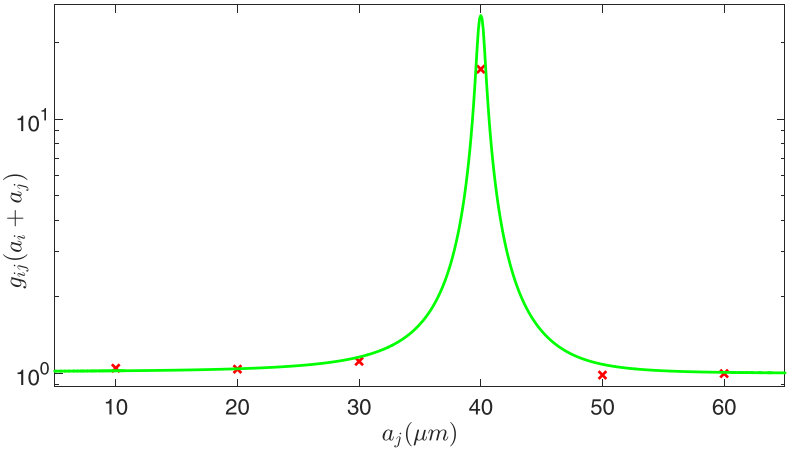

FIG. 5. The RDF of particles at contact $g_{ij}(a_i + a_j)$ is plotted as a function of a_j, with $a_i = 40$ μm. This corresponds to a variation of St_j in the approximate range of 0.05 to 2. The DNS data [1], calculated at $\epsilon = 0.04$ m^2/s^3 and $\mathrm{Re}_\lambda = 72.41$, is shown with symbols, while the solid lines show the results of our model. The errors are minimal at all points of comparison.

Increasing $\Delta S_{v,ij}$ to 4/3 significantly decreases the value to which the RDF plateaus by about a factor of 3 even though based solely on mean St this case is expected to show higher clustering. The St dependence can be observed when $\Delta S_{v,ij} = 1/3$ but larger $g_{ij}(r)$ is seen when the mean St is closer to one. It should be noted that in our model the dominant contribution of the size ratio appears through differential sedimentation, that scales as $\Delta S_{v,ij}$. The only other term that contains size ratio is $D_{||,\epsilon,ij}$ and it is much smaller than $D_{||,g,ij}$ or $B_{||}$.

The variation of the RDF with St and $\Delta S_{v,ij}$ has been accurately resolved in our inertial clustering model. This will be crucial in predicting concentration enhancement during collision of two particles. To demonstrate the accuracy of the inertial clustering model predictions, we consider water droplets in clouds. For these micron-sized droplets, Ayala *et al.* [1] have performed DNS calculations to determine the RDF at contact, i.e., $g_{ij}(a_i + a_j)$, of noninteracting particles for a turbulent dissipation rate $\epsilon = 0.04 m^2/s^3$ and Taylor-scale Reynolds number $\mathrm{Re}_\lambda = 72.41$. This dissipation rate corresponds to $\mathrm{Fr} = 0.14$. We compare with these DNS results by fixing a_i at 40 μm and varying a_j from 5 to 65 μm in Fig. 5. Due to the low value of Re_λ we use the correction given in Eq. (6), though it will not alter the results at such small particle separations. We find good agreement between our model results and DNS data on the decay of inertial clustering as the particle sizes become disparate and differential sedimentation decorrelates the clusters. The deviation for the monodisperse data point is also minimal, highlighting the weak effect gravity has on inertial clustering of equal sized particles at moderately large Fr and justifying our neglect of this mechanism.

Evaluation of the RDF in Eq. (16) requires a combination of dimensional parameters such as the radii, ρ_p, ϵ, ν, and g and the nondimensional quantity Re_λ. From these the important nondimensional parameters such as St, Fr, and $\Delta S_{v,ij}$ can be obtained. Our results are fairly accurate over St from 0.05 to 30 which is the range over which DNS data is available. The deviations of the predictions from DNS $g(r) - 1$ is at most 7% in the critical dissipative sizes and inertial subrange. Outside of these ranges there are very limited theoretical insights that can be incorporated into our model. We have tackled the transition from dissipative to integral scale at low Re_λ, where there is no inertial subrange, to better compare with RDF data available in literature. However, the model is most accurate at high Re_λ and η/a where there are extended inertial and dissipative ranges. In the transition between these two ranges, at high Re_λ, we find deviations of less than 12%. The differential sedimentation metric $\Delta S_{v,ij}$ has been tested to values as high as 4/3 and

we find the largest difference from DNS to be about 13%. For Fr there is a paucity of data but our model assuming infinite Froude number has been tested against values of the Froude number as low as 0.052 showing deviations of about 18%. The estimate for $\mathrm{Fr} = 0.3$ can be made from Fig. 4 where the errors are only about 13% in spite of confounding factors such as bidispersity.

The inertial clustering model presented here is valid over a large range of St and $\Delta S_{v,ij}$. The RDF can be evaluated from this model by performing the numerical integral in Eq. (16) with orders of magnitude less computational effort than a DNS study. However, the model might be slower than would be desirable when computing the evolution of the drop size distribution. Hence, in the Appendix we develop a simplified model for $g_{ij}(r)$ that yields a closed form expression.

III. COMPARISON WITH EXPERIMENTAL MEASUREMENTS

In this section we will use the model developed in Sec. II to predict inertial clustering observed in experiments. Each experimental study only explores a limited region of the large parameter space spanned by the model. Hence, we will draw from multiple experimental studies [16–19].

To compare with experiments, we assume that the measurements are performed in a region of the suspension that is well mixed and has reached a statistical steady state. We assume that the flow outside the region of homogeneous turbulence does not affect the RDF within this well mixed region. The Reynolds number based on particle radius and settling velocity is assumed to be small and we assume that $a \ll \eta$ so that gas inertia associated with turbulent shear on the particle scale can be neglected. The particles are treated as points and this is valid for $r \gg a$. All of these assumptions are satisfied for the experiments considered in this section except that r becomes comparable with a for the smallest separation experiments of Yavuz *et al.* [19] and the suspension studied by Ref. [17] is not well mixed on the integral and inertial subrange scales. The theoretical and numerical treatment of clustering focuses on the turbulent fluid motion, particle inertia and gravitational settling but neglects colloidal interactions such as van der Waals and electrostatic forces. In the available experimental studies the discussion and the reported error analysis do not consider such interactions as a significant source of clustering. Hence, we do not consider them here.

The model described above yields the pair distribution function g_{ij} of particle pairs with different size. In this section we will use the $g_{ij}(r)$ that includes the correction for small separations of turbulent length scales, given by Eq. (6), since most experiments are performed at low Re_λ. While some experiments aim to produce nearly monodisperse suspensions, even the most carefully designed experiments will possess some spread in the distribution of the particle sizes. To account for this we average the RDF over the reported experimentally measured size distribution of the particles, yielding an overall pair probability $g^*(r) = \int g_{ij}(r)P(a_i)P(a_j)da_i da_j$. Here $P(a)$ is the probability of finding a particle of radius a. Saw *et al.* [17] report their experimental results using bins of Stokes number, with the RDF generated from the particles in the same bin considered approximately monodisperse and those from different bins presented as the approximate bidisperse pair distribution function g^*_{ij}. Our predictions for these are obtained by performing a similar integral with the limits of integration on a_i and a_j limited to restricted regions over which the experimental measurements were binned.

The RDF of silver-coated hollow-glass spheres in a turbulent air chamber has been observed by Salazar *et al.* [16]. They performed measurements for three turbulence levels and we compare with each of them in Fig. 6. Our predictions use their reported particle size distribution, with a mean and standard deviation of 3 and 2 μm, respectively, that excludes particles below a radius of 2.5 μm. This high pass filter mimics the small particles that have been reported to be missed by the camera used in the experiment. There is relatively good agreement between the output of our model and experimental data at small separations. The largest deviation in $g^*(r) - 1$ is about 20% and is observed at the lowest dissipation rate. This has been flagged in the original experimental paper as a noticeable under-prediction by DNS without any satisfactory explanation. Hence, we do not attempt

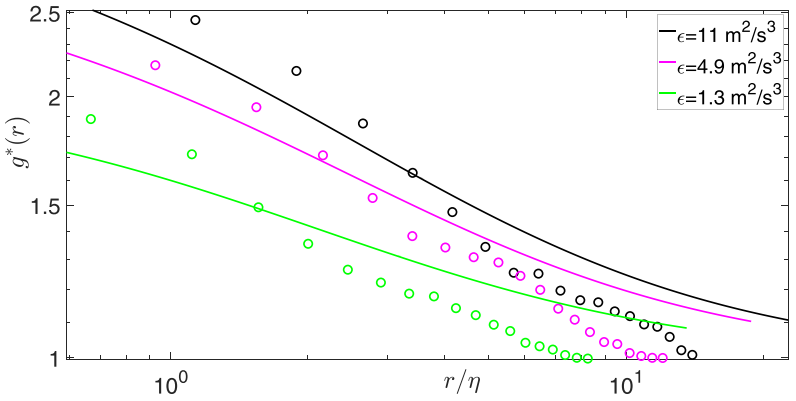

FIG. 6. The averaged pair probability $g^*(r)$ is plotted as a function of r/η, with symbols corresponding to the experimental data from Salazar *et al.* [16] and solid lines the predictions by our model. Here $\epsilon = 1.33,\ 4.9,\ 11\ \mathrm{m}^2/\mathrm{s}^3$ corresponds to Re_λ of 108, 134, 147 and mean $\mathrm{St} = 0.08,\ 0.13,\ 0.2$.

to resolve the similar under-prediction of the experiments by our model. At the higher dissipation rates the deviations at small separations are much smaller. At large separations the experimentally measured $g^*(r)$ rapidly falls off. This is likely due the experimental errors introduced by the finite measurement window of about 1 cm^3.

Higher Re_λ than those considered in Ref. [16] are more typical in real world turbulent flows, such as atmospheric clouds [26]. A more realistic Re_λ, of 440, has been achieved in the experimental study by Saw *et al.* [17]. They measured inertial clustering of water droplets in a wind tunnel. The Stokes numbers of these droplets were found to follow a log-normal distribution and the RDF has been calculated by binning measurements over a certain range. The binning allows them to look at nearly bidisperse particle collisions and so is relevant to test our inertial clustering model dependence on size differences. This comparison is shown in Fig. 7 for experimental conditions corresponding to $\epsilon = 0.6\ \mathrm{m}^2/\mathrm{s}^3$ and $\mathrm{Re}_\lambda = 440$. Good qualitative agreement is found between the predictions of our model and experimental data even though differential sedimentation, the primary focus of the bidisperse modeling in the present study, plays a small role in these experiments. In particular, the trends of the RDF with St and r in the experiments are reproduced by the model. A

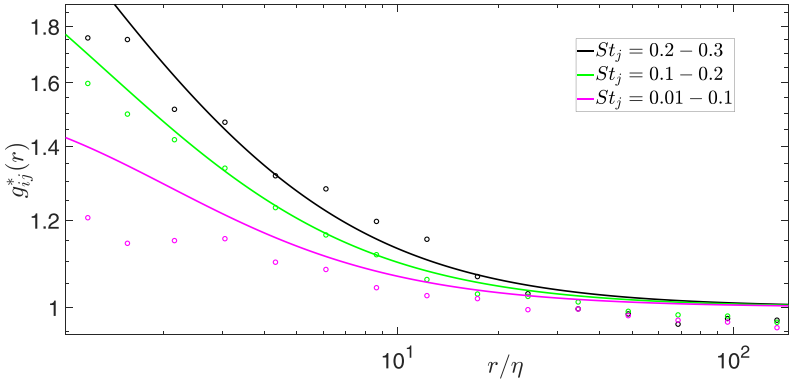

FIG. 7. Comparison against the experiments by Saw *et al.* [17] (symbols) performed at $\epsilon = 0.6\ \mathrm{m}^2/\mathrm{s}^3$ and $\mathrm{Re}_\lambda = 440$ against our averaged g^*_{ij} (solid lines) is shown as a function of r/η. The binning of the reported size distribution is done with $\mathrm{St}_i = 0.2$–0.3 and three different St_j of 0.2–0.3, 0.1–0.2, and 0.01–0.1, thus capturing a nearly monodisperse case as well as two bidisperse cases.

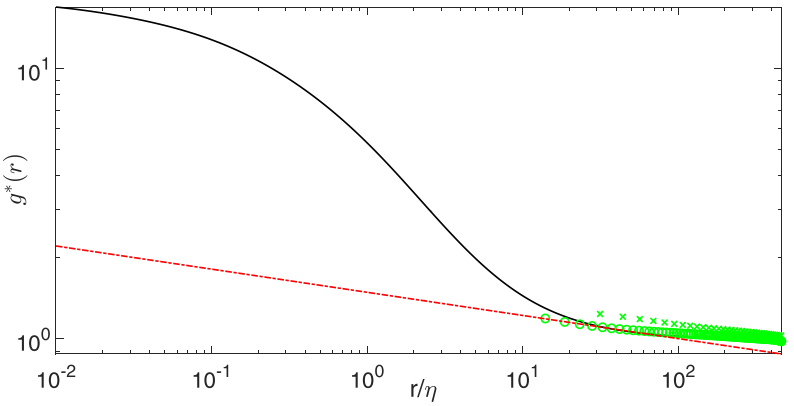

FIG. 8. For $\mathrm{Re}_\lambda = 300$, $\mathrm{Fr} = 1.2$, mean $\mathrm{St} = 0.63$, and $\eta = 0.27$ mm $g^*(r)$ is shown as a function of r/η. The symbols and dash-dotted red line are experimental measurements by Petersen *et al.* [18] and a fit suggested by these authors, respectively. The symbols "x" and "o" are the experiments performed under the same conditions but measured with a lower and higher field of view respectively. There is a larger difference between these measurements than between our model's result (shown with the black line). However, our model predicts much stronger clustering at smaller separations than suggested by the fit.

complication in this experiment was that the particles were not well mixed on the inertial subrange scales. To account for this, the authors assumed that the effects of transient mixing on the inertial subrange scale and preferential concentration on the dissipative scale were independent processes. The experimental RDF reported in Fig. 7 is shifted to remove the mixing effects. This process would not properly account for the preferential concentration that occurs in the inertial subrange. In addition, it should be noted that the asymptotic theory for low Stokes number [3] suggests that dissipative scale preferential concentration is influenced by the temporal evolution of the dissipation rate and enstrophy which evolve on the inertial timescales. Uncertainties associated with the effort to disentangle mixing and preferential concentration may account for the low values of the adjusted experimental RDF for the smallest St_j at all r and for all St_j at large r/η. Excluding those the highest $g^*(r) - 1$ deviation is about 20%.

In contrast to the rest of the experimental results considered here, which have implicitly assumed infinite Fr, Petersen *et al.* [18] performed experiments with a moderate Fr for which gravity may play a role. They study particles experiencing turbulence through an array of jets and reach $\mathrm{Fr} \approx 1$ and S_v as high as 8. Unfortunately, they only test nearly equal sized particles and so the plateauing of the pair distribution function due to differential sedimentation, that can be estimated to occur when $\Delta S_{v,ij}\eta/r$ is order one, lies well within the dissipative range and beyond the range observed in the experiment. Still our model is expected to perform well in the reported separation range as we have already argued that the role of gravity on the inertial clustering of a monodisperse distribution of particles at moderate Froude numbers is minimal. We compare with their experiments on Lycopodium particles whose radii have a mean and standard deviation of 15 and 1 μm, respectively, and assume a Gaussian distribution for the particle radius distribution. The flow conditions correspond to $\mathrm{Fr} = 1.2$, $\mathrm{Re}_\lambda = 300$, and a Kolmogorov length scale of 0.27 mm, leading to a mean St of 0.63. For this case, the reported fit of the experimental data, uses a function based on the power-law behavior expected in the dissipative range. We show this, along with the experimental data and the results of our model, in Fig. 8. To show the robustness of our model, in addition to the data, the experimental error bounds are needed. To obtain this we plot the experimental data obtained from measurements with a large and small field of view. The deviation between these is greater than the difference between our model prediction and so we conclude a good agreement has been achieved. However, in view of the large Stokes number, the model predicts that a much higher pair distribution function would be observed in the

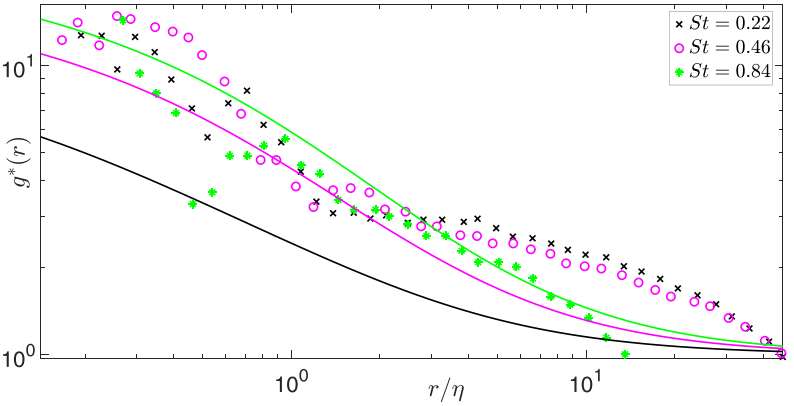

FIG. 9. The averaged RDF $g^*(r)$ is shown as a function of r/η. The symbols are the experimental data from Yavuz *et al.* [19] while the solid lines are the predictions of our inertial clustering model. We compare against three experiments with mean St $= 0.22,\ 0.46,\ 0.84$, mean radii of $7.1,\ 10,\ 20.7$ μm and standard deviations of $0.3,\ 0.6,\ 0.7$ μm, respectively. The flow condition for the first two correspond to $\epsilon = 2.1$ m^2/s^3 and $\mathrm{Re}_\lambda = 229$ while the last one is at $\epsilon = 0.3$ m^2/s^3 and $\mathrm{Re}_\lambda = 155$. The experiments do not exhibit a consistent physically expected variation with St.

dissipation range than suggested by a simple power-law fit. Eventually the model predicts a plateau of the pair distribution function when differential sedimentation becomes important at separations smaller than about 0.2η. This comparison illustrates the value of using a comprehensive model to identify the dominant physics controlling the pair distribution function in the range of experimental measurements.

To observe the largest enhancements of the pair distribution function due inertia, it would be desirable to perform measurements at sub-Kolmogorov separations. This was attempted by Yavuz *et al.* [19] who studied water droplets in a soccer-ball-shaped chamber with turbulence produced by a collection of loudspeakers. In Fig. 9, we compare with their measurements for three experiments, computing $g^*(r)$ by assuming a Gaussian distribution for the droplet radii defined by the reported mean and standard deviation. Although the experimentally measured pair distributions for the two large Stokes numbers are comparable in magnitude to the predictions in the sub-Kolmogorov range, the experiments and model are otherwise in poor agreement, with deviations as high as 70%. However, there are some issues immediately evident in the experimental data. At all separations the reported RDF fails to grow with St for St < 1. This is contrary to current physical understanding of the origins of clustering and contradicts other experiments performed with similar values of St [16,17]. At small particle separations the experimental data is nearly collapsed for the three St shown. This corresponds to a significantly higher than expected $g^*(r)$ when the lowest St experimental result is considered and, presently, there is no known physical mechanism to account for such a dramatic enhancement. Hydrodynamic interactions were shown by Brunk *et al.* to enhance inertial clustering only by an $O(1)$ factor [27]. This would be insufficient to account for the order of magnitude increase of $g^*(r)$. A recent paper by Bragg *et al.* [28] provides further experimental measurements indicating a rapid increase in the RDF at separations comparable with the particle radius along with an analysis showing that this increase cannot be attributed to any known hydrodynamic or colloidal particle interaction mechanisms or the current understanding of inertial particle dynamics in turbulence.

IV. APPLICATION TO INERTIAL ENHANCEMENT OF CLOUD DROPLET COALESCENCE

In Sec. II we have developed a model for the pair distribution $g(r)$ in a polydisperse suspension resulting from particle inertia, turbulence, and differential sedimentation and this model was

compared with multiple experimental studies in Sec. III. This inertial clustering model will inform the effective collision rate experienced between particle pairs. To demonstrate this, in this section, we consider atmospheric clouds, where collisions driven by turbulence and gravitational settling are both expected to be important for micron-sized droplet growth. Utilizing these results we will analyze how the critical parameters shape inertial clustering and by extension the expected collision rate in clouds.

Cloud droplet evolution for droplets of radii 15 to 40 μm is an active area of research in climate science. Referred to as the "size-gap," it is a range in which differential sedimentation and condensation growth are weak and it is not fully understood how droplets grow [26]. Inaccurate models in this regime lead to significant deviations between prediction and observation. *In situ* measurements of drop size distribution in clouds and the time to precipitation, which is sensitive to droplet growth in the size-gap do not agree with current models. Many mechanisms have been proposed to resolve these discrepancies including turbulent collisions [29], polydispersity induced by mixing [30], and ultragiant condensation nuclei [31], to name only a few. Studies, such as that by Vaillancourt *et al.* [32], have investigated the role of inertial clustering driven enhancement of the collision rate in crossing the "size-gap" and we will focus on this mechanism in this section. We will use our inertial clustering model that accurately resolves how particle inertia driven clustering occurs under the coupled action of turbulence and differential sedimentation.

Inertial clustering plays an important role influencing the observed collision rate of droplets in clouds [1]. However, it is beyond the scope of this study to do a full simulation of the evolution of the drop size distribution and so we will only calculate the effective collision rate experienced by a distribution of droplets. We will span the mean radius a_m from 15 to 40 μm corresponding to the critically important "size-gap." To capture polydispersity, and thus the influence of differential sedimentation, we assume a Gaussian distribution and vary the standard deviation σ_a from 0.01 to 1.5 μm. The sedimentation induced relative velocity of two particles can be impacted by particle inertia and its role can be estimated using $\mathrm{St}_g = 2U_{\mathrm{rel}}(4\rho_p\pi/3)\sqrt{a_1^3 a_2^3}/\mu(a_1+a_2)^2$ (see Davis [33]). A St_g of less than 1.9 has been estimated to be sufficient to approximate the gravity-driven collision rate with its inertialess value [20].

While droplet inertia based on the turbulent timescale and the mean droplet size is not negligible in the size gap, estimates by Chun *et al.* and Ireland *et al.* [3,10] showed that, when $\mathrm{St} < 0.2$, inertia does not alter the local collision dynamics and only enhances the collision rate through inertial clustering leading to droplets being more likely to encounter each other. This can be expressed as

$$K_{ij} = g_{ij}(a_i + a_j)K_{ij}^0. \tag{18}$$

Here, K_{ij} is the actual collision rate between species i and j while K_{ij}^0 is the collision rate without particle inertia computed by Dhanasekaran *et al.* [20], who evaluated the collision rate of drops due to the coupled effects of turbulence and differential sedimentation in the presence of noncontinuum lubrication and long-range continuum hydrodynamic interactions. For the assumed Gaussian distribution we obtain the effective collision rates without (K^0) and with inertial clustering (K) as

$$K^0 = \int K_{ij}^0 P(a_i)P(a_j)da_i da_j, \tag{19}$$

$$K = \int g_{ij}(a_i + a_j)K_{ij}^0 P(a_i)P(a_j)da_i da_j. \tag{20}$$

To obtain the collision rates we assume conditions typical in clouds, of $\epsilon = 0.01\ \mathrm{m}^2/\mathrm{s}^3$, mean free path of air of 70 nm, and $\mathrm{Re}_\lambda = 2500$. The integrals in Eqs. (19) and (20) are performed by Monte Carlo integration by choosing 100 particle pairs from the Gaussian distribution of droplet radii. The impact of the enhancement is visualized in a color plot K/K^0 in Fig. 10 as a function of a_m and σ_a. To better contextualise the plot, we include two constant-Stokes-number curves: $\mathrm{St} = 0.2$ (green) and $\mathrm{St}_g = 1.9$ (black) for reference. Below the St and St_g constant curves the use of Eq. (18)

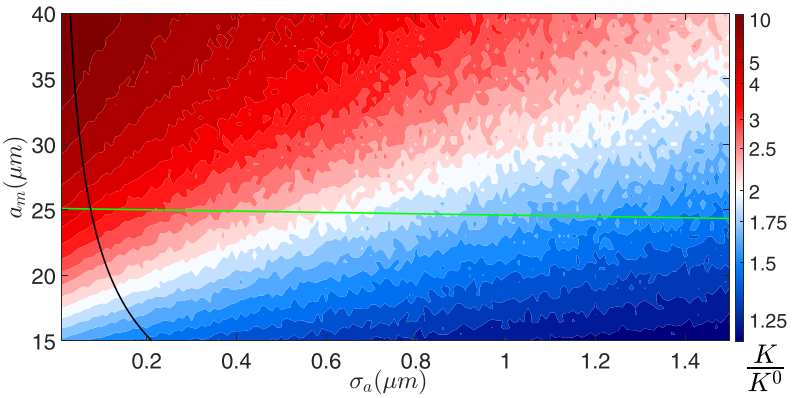

FIG. 10. A color plot of the enhancement of collision rate, K/K^0, due to preferential concentration as a function of the mean and standard deviation of the radius, a_m and σ_a. Significant enhancement due to $g(r)$ is observed across the parameter space but the strongest effect occurs for nearly monodisperse collisions and larger sizes within the "size-gap." To gauge the values of the relevant nondimensional numbers curves of constant St $= 0.2$ (green) and $\mathrm{St}_g = 1.9$ (black) are included.

is valid and the assumption that inertia does not alter the gravitational relative velocity is accurate. In the broader region we can gain important qualitative insight into the role of inertial clustering on droplet evolution within the "size-gap" regime.

The enhancement observed is more than 25% over most of the parameter regime shown here indicating that inertial clustering will have a major impact of the collisional growth. To contextualise, the mean radius spans the "size-gap" and the typical size ratio, characterized by σ_a/a_m, considered here only goes as high as 0.1. This modest polydispersity is not unusual for condensation controlled size distribution formed at the beginning of the size-gap. The enhancement within this critical region is complex, with competing effects of increasing polydispersity and size. As a_m increases it is expected that the collision rate increases but within the "size-gap" so does its enhancement due to inertial clustering. This can be understood by the RDF being monotonically related to Stokes number when it is not too large, which holds under the present conditions for which St ranges from 0.07 to 0.51. Polydispersity might be expected to be weak given the small size ratio but it drives a sharp drop in K/K^0 with increasing size ratio. Hence, the broader distribution generated by collisional growth will experience a much weaker boost due to inertial clustering highlighting the highly "focused" manner in which it acts. In the monodisperse environment at the end of the period of condensation dominated droplet growth, inertia driven preferential concentration can significantly enhance the probability of collisional growth to sizes larger than 15 μm and promote polydispersity. In the "size-gap" increasing droplet size competes with higher size variation in setting the strength of inertial clustering and so it cannot be be discounted until the growth phase fuelled by differential sedimentation driven collisions is reached. Hence, inertial clustering will be crucial in shaping the evolution of the drop size distribution. Consequently, the results of our study are expected to be integral to a detailed drop evolution simulation.

Due to turbulent intermittency it is possible to experience a dissipation rate higher than the ϵ chosen here. For an order of magnitude $\epsilon = 0.1$ m^2/s^3 we have Fr $= 0.3$ for which our model has been showed to be valid. Hence, a plot similar to Fig. 10 can be generated. For the sake of brevity we will not span the dissipation parameter space. Instead we note that even in this highly turbulent condition St within the size-gap only goes as high as 1.6 and so the peak clustering as function of Stokes number is not yet expected to be reached. Thus, all the qualitative insights obtained are expected to hold.

V. SUMMARY

We have developed a model for inertial clustering of particles settling in a turbulent flow. It incorporates known asymptotic results, such as the power-law dependence of the RDF of monodisperse particles on radial position in the dissipative range. Bidispersity is treated and differential sedimentation attenuates the accumulation of particle pairs due to inertial drift. The unknown constants, due to the limits of available analytical results and the approximate nature of our treatment of differential sedimentation, are determined from DNS studies of monodisperse and bidisperse particles. Our predictions agree well with DNS and experimental data for both monodisperse and bidisperse cases. We use our model to study the impact on the coalescence rate of micron-sized droplets in clouds. This analysis highlights the intricate details of how the parameters, such as the drop size and size difference, impact clustering.

In Sec. II, we developed a model to accurately predict the RDF over a wide range of St and r. The model is valid over a moderate range of bidispersity and Fr. We provided an approximation for the RDF of a monodisperse dispersion without gravity over all length scales using known asymptotic limits and DNS data to incorporate behavior for which simple theoretical expressions are not available, such as the nonlocal movement of particles between eddies. This result is used to predict the inward drift of an equivalent bidisperse particle pair that counteracts turbulent shear diffusion coupled with a model for decorrelation due to differential sedimentation. Gravitational effects on bidisperse particles are treated as an effective diffusivity motivated by the concept that the turbulent shear allows particle pairs to experience a distribution of angles between the particle separation vector and gravity. The solution of this drift-diffusion equation gives $g(r)$. The order one free parameter, embedded within the diffusion model, is obtained by fitting to available DNS data[12]. The accuracy of our $g(r)$ is demonstrated by comparing $g(a_1 + a_2)$ with DNS data [1] available over a range of sizes. Our model holds for weak gravitational sampling (scaling as S_v) which can still generate strong differential sedimentation (scaling as $\Delta S_{v,ij}\eta/[a_1 + a_2]$).

The model for clustering is compared with available experimental results in Sec. III. The comparisons take account of the reported polydispersity in the experiments. Good agreement is found with low Re_λ nearly monodisperse experimental data [16], with errors around 20%, as well as those performed at higher Re_λ and reporting $g_{ij}(r)$ on bidiperse slices of a size distribution [17], with our predictions deviating by about 20%. Inertial clustering measurements, with moderate Froude number and moderately high Re_λ of 300 [18], are consistent with our RDF, which show deviations smaller than experimental error estimates. However, the predicted $g(r)$ rises to much larger values within the dissipative subrange than would be expected from the simple fit presented along with the experimental data [18]. We also show that differential sedimentation would significantly alter this RDF at sub-Kolmogorov distances. These comparisons highlight two limitations of currently available experimental results. First, few results are available at sub-Kolmogorov separations where the greatest inertial clustering is predicted to occur. Those measurements that are available are not consistent with the current understanding of inertial particle dynamics in turbulence and particle interaction mechanisms [19,28]. Second, no measurements are available to assess the manner in which differential sedimentation attenuates inertial clustering.

Having developed and tested our model we apply it to predict the coalescence of micron-sized droplets in clouds in Sec. IV by assuming that inertia, for the relevant cloud conditions, only impacts the local pair probability. Inertial clustering is found to significantly enhance the effective collision rate within the "size-gap" where droplet growth is slowest. While the larger drops collide more due to their higher RDF's, the increase in collision rate is appreciable throughout the 15–40 μm water droplet size range. Although this enhancement decays rapidly as the standard deviation of the drop size distribution increases, it may play a crucial role in generating polydispersity and enhancing the sedimentation driven coalescence rate. These results illustrate the importance of inertial clustering modeling that incorporates the effect of differential sedimentation to accurately model the evolution of the droplet size distribution.

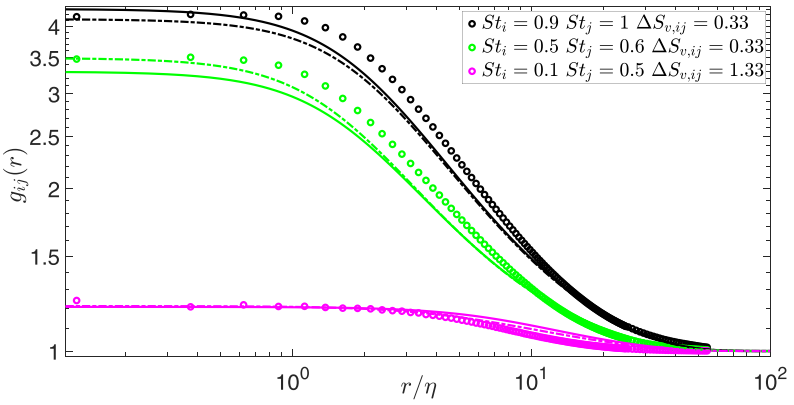

FIG. 11. $g_{ij}(r)$ is shown as a function of r/η for three bidisperse calculations performed at $\mathrm{Re}_\lambda = 90$ and $\mathrm{Fr} = 0.3$. The symbols denote DNS data [12] and the solid lines are the predictions of the algebraic model of inertial clustering shown in Eq. (11). For reference the results from Fig. 4, obtained from our model described in Sec. II, are shown with dashed-dotted lines. Good agreement is observed across the parameter space.

ACKNOWLEDGMENTS

This work was supported by NSF Grants No. 1435953 and No. 2206851.

APPENDIX: ALGEBRAIC MODEL FOR INERTIAL CLUSTERING

The inertial clustering result presented in Eq. (16) requires integrating the radial flux balance of drift and diffusion across separations spanning the many scales of turbulence. While this is dramatically faster than obtaining $g_{ij}(r)$ from a DNS calculation, it might still prove to be a stumbling block for calculations of an evolving drop size distribution where the RDF is required for a broad range of parameters. Hence, a closed form algebraic expression for $g_{ij}(r)$ is derived. It is motivated by the idea of a cut off radius r_c representing the transition from monodispere power-law behavior at larger separations to a flattening of the RDF due to bidispersity when the particle pairs are close to each other [3]. This is given as

$$g_{ij}(r) = c_0 \left(\frac{\eta^2 + r_c^2}{\eta^2 + r^2} \right)^{c_1/2}. \tag{A1}$$

While this result is exact for small St and $r \ll \eta$ in the absence of gravity a similar result was postulated for bidisperse spheres driven by turbulence and differential sedimentation at separations in the dissipative range [15]. To allow the cut off radius to occur for any r, we introduce it into the uniformly valid monodisperse result of Eq. (3) and obtain

$$g_{ij}(r) = \exp\left(\frac{\log c_0}{\left(1 + \frac{\sqrt{r^2+r_c^2}}{2\eta\left(1+\left(\frac{\mathrm{St}_i+\mathrm{St}_j}{2}\right)^{3/2}\right)}\right)^{\frac{4}{3}}} \right) \left(1 + \frac{\eta}{\sqrt{r^2+r_c^2}}\right)^{c_1}. \tag{A2}$$

Here, c_0 and c_1 are evaluated at $\mathrm{St} = \frac{\mathrm{St}_i+\mathrm{St}_j}{2}$. The characteristic separation r_c sets the crossover from monodisperse behavior to the bidisperse plateau of $g_{ij}(r)$. This crossover length is set by the competition between the characteristic settling and turbulent velocities and is given as

$$r_c = k_c g |\mathrm{St}_i - \mathrm{St}_j| \sqrt{15\tau_\eta^2}. \tag{A3}$$

Here k_c is independent of r and, similar to the integral model, is obtained by fitting with DNS results [12] and determined to be

$$k_c = 1 + 5\frac{\mathrm{St}_i + \mathrm{St}_j}{2}|\mathrm{St}_i - \mathrm{St}_j|. \tag{A4}$$

The algebraic model for inertial clustering is compared with DNS results [12] in Fig. 11. These were carried out at $\mathrm{Fr} = 0.3$ and $\mathrm{Re}_\lambda = 90$ and so the correction for small Re_λ given in Eq. (6) is needed for large particle separations. From the figure it is evident that all the important features of the RDF, including variation with r, St, and $\Delta S_{v,ij}$, have been captured with reasonable accuracy.

[1] O. Ayala, B. Rosa, L.-P. Wang, and W. Grabowski, Effects of turbulence on the geometric collision rate of sedimenting droplets. Part 1. Results from direct numerical simulation, New J. Phys. **10**, 075015 (2008).

[2] L. Pan, P. Padoan, J. Scalo, A. G. Kritsuk, and M. L. Norman, Turbulent clustering of protoplanetary dust and planetesimal formation, Astrophys. J. **740**, 6 (2011).

[3] J. Chun, D. L. Koch, S. L. Rani, A. A, and L. R. Collins, Clustering of aerosol particles in isotropic turbulence, J. Fluid Mech. **536**, 219 (2005).

[4] A. D. Bragg, P. J. Ireland, and L. R. Collins, Mechanisms for the clustering of inertial particles in the inertial range of isotropic turbulence, Phys. Rev. E **92**, 023029 (2015).

[5] L. I. Zaichik and V. M. Alipchenkov, Pair dispersion and preferential concentration of particles in isotropic turbulence, Phys. Fluids **15**, 1776 (2003).

[6] H. Xu and E. Bodenschatz, Motion of inertial particles with size larger than Kolmogorov scale in turbulent flows, Physica D **237**, 2095 (2008).

[7] L. I. Zaichik and V. M. Alipchenkov, Refinement of the probability density function model for preferential concentration of aerosol particles in isotropic turbulence, Phys. Fluids **19**, 113308 (2007).

[8] L. I. Zaichik and V. M. Alipchenkov, Statistical models for predicting pair dispersion and particle clustering in isotropic turbulence and their applications, New J. Phys. **11**, 103018 (2009).

[9] P. Ireland, A. Bragg, and L. Collins, The effect of reynolds number on inertial particle dynamics in isotropic turbulence. Part 1. Simulations without gravitational effects, J. Fluid Mech. **796**, 617 (2016).

[10] P. Ireland, A. Bragg, and L. Collins, The effect of Reynolds number on inertial particle dynamics in isotropic turbulence. Part 2. Simulations with gravitational effects, J. Fluid Mech. **796**, 659 (2016).

[11] A. D. Bragg and L. R. Collins, New insights from comparing statistical theories for inertial particles in turbulence: I. Spatial distribution of particles, New J. Phys. **16**, 055013 (2014).

[12] R. Dhariwal and A. Bragg, Small-scale dynamics of settling, bidisperse particles in turbulence, J. Fluid Mech. **839**, 594 (2018).

[13] S. L. Rani, V. K. Gupta, and D. L. Koch, Clustering of rapidly settling, low-inertia particle pairs in isotropic turbulence. Part 1. Drift and diffusion flux closures, J. Fluid Mech. **871**, 450 (2019).

[14] O. Ayala, B. Rosa, and L.-P. Wang, Effects of turbulence on the geometric collision rate of sedimenting droplets. Part 2. Theory and parameterization, New J. Phys. **10**, 075016 (2008).

[15] J. Lu, H. Nordsiek, and R. A. Shaw, Clustering of settling charged particles in turbulence: Theory and experiments, New J. Phys. **12**, 123030 (2010).

[16] J. P. Salazar, J. De Jong, L. Cao, S. H. Woodward, H. Meng, and L. R. Collins, Experimental and numerical investigation of inertial particle clustering in isotropic turbulence, J. Fluid Mech. **600**, 245 (2008).

[17] E.-W. Saw, R. A. Shaw, J. P. Salazar, and L. R. Collins, Spatial clustering of polydisperse inertial particles in turbulence: II. Comparing simulation with experiment, New J. Phys. **14**, 105031 (2012).

[18] A. J. Petersen, L. Baker, and F. Coletti, Experimental study of inertial particles clustering and settling in homogeneous turbulence, J. Fluid Mech. **864**, 925 (2019).

[19] M. A. Yavuz, R. P. J. Kunnen, G. J. F. Van Heijst, and H. J. H. Clercx, Extreme Small-Scale Clustering of Droplets in Turbulence Driven by Hydrodynamic Interactions, Phys. Rev. Lett. **120**, 244504 (2018).

[20] J. Dhanasekaran, A. Roy, and D. L. Koch, Collision rate of bidisperse, hydrodynamically interacting spheres settling in a turbulent flow, J. Fluid Mech. **912**, A5 (2021).
[21] W. C. Reade and L. R. Collins, Effect of preferential concentration on turbulent collision rates, Phys. Fluids **12**, 2530 (2000).
[22] S. L. Rani, R. Dhariwal, and D. L. Koch, Clustering of rapidly settling, low-inertia particle pairs in isotropic turbulence. Part 2. Comparison of theory and DNS, J. Fluid Mech. **871**, 477 (2019).
[23] L. I. Zaichik, O. Simonin, and V. M. Alipchenkov, Collision rates of bidisperse inertial particles in isotropic turbulence, Phys. Fluids **18**, 035110 (2006).
[24] L. Pan and P. Padoan, Turbulence-induced relative velocity of dust particles. I. Identical particles, Astrophys. J. **776**, 12 (2013).
[25] R. Dhariwal, S. L. Rani, and D. L. Koch, Stochastic theory and direct numerical simulations of the relative motion of high-inertia particle pairs in isotropic turbulence, J. Fluid Mech. **813**, 205 (2017).
[26] W. W. Grabowski and L.-P. Wang, Growth of cloud droplets in a turbulent environment, Annu. Rev. Fluid Mech. **45**, 293 (2013).
[27] B. Brunk, D. Koch, and L. Lion, Hydrodynamic pair diffusion in isotropic random velocity fields with application to turbulent coagulation, Phys. Fluids **9**, 2670 (1997).
[28] A. D. Bragg, A. L. Hammond, R. Dhariwal, and H. Meng, Hydrodynamic interactions and extreme particle clustering in turbulence, J. Fluid Mech. **933**, A31 (2022).
[29] A. B. Kostinski and R. A. Shaw, Fluctuations and luck in droplet growth by coalescence, Bull. Am. Meteorol. Soc. **86**, 235 (2005).
[30] S. G. Lasher-trapp, W. A. Cooper, and A. M. Blyth, Broadening of droplet size distributions from entrainment and mixing in a cumulus cloud, Quart. J. R. Meteorol. Soc. **131**, 195 (2005).
[31] S. G. Lasher-Trapp, C. A. Knight, and J. M. Straka, Early radar echoes from ultragiant aerosol in a cumulus congestus: Modeling and observations, J. Atmos. Sci. **58**, 3545 (2001).
[32] P. Vaillancourt, M. Yau, P. Bartello, and W. W. Grabowski, Microscopic approach to cloud droplet growth by condensation. Part II: Turbulence, clustering, and condensational growth, J. Atmos. Sci. **59**, 3421 (2002).
[33] R. Davis, The rate of coagulation of a dilute polydisperse system of sedimenting spheres, J. Fluid Mech. **145**, 179 (1984).